Supplementary information for:

Dry hydroclimates in the late Palaeocene-early Eocene hothouse world

Victor A. Piedrahita[1,2,3,4], Andrew P. Roberts[4], Eelco J. Rohling[5,6], David Heslop[4], Xiang Zhao[4], Simone Galeotti[7,8], Fabio Florindo[8,9], Katharine M. Grant[4], Pengxiang Hu[4], Jinhua Li[1,2,3,10]

Supplementary results

X-ray fluorescence

Detrital elements (Fe, Rb, Si, Ti, and Zr) increase in coincidence with Ca reductions, which reveals $CaCO_3$ dissolution and confirms that $CaCO_3$ variability is the main sedimentation mechanism at the Contessa Road section[1-3] (Fig. S3a-f). Sr, which can be either fixed by calcifying organisms or incorporated into terrigenous minerals[4], does not follow a consistent pattern with either Ca or detrital elements (Fig. S3). From principal component analysis (PCA; Fig. 6b), Sr is not associated clearly with either terrigenous or biogenic sedimentation at Contessa Road, so we interpret its variability to have been controlled by both sedimentation types. Sr contributions to $PC1_{all}$ and $PC2_{all}$ are small, as indicated by its loading (Fig. 6b); hence, sedimentation patterns identified by PCA_{all} are not modified significantly by Sr variability.

Rock magnetism

Magnetic mineral unmixing (see Methods) was performed to verify that the hard isothermal remanent magnetization (HIRM) and anhysteretic remanent magnetization (ARM) do not underestimate or overestimate high coercivity and low coercivity magnetic mineral contents[5].

Hence, isothermal remanent magnetization (IRM) distributions were used only to separate high and low coercivity magnetic mineral assemblages (left column in Fig. S10 in the main text). IRM distributions allow clear identification of a high coercivity component that is interpreted to consist mainly of haematite, although it contains goethite during the early Eocene low magnetization zone (EELMZ). A main low coercivity component (referred to as low coercivity component 1) is also clearly identified and related to maghemite and magnetite. A secondary small low coercivity component appears in some samples and may also be associated with detrital minerals (left column in Fig. S10).

Early Palaeogene Contessa Road magnetic mineral assemblages have been indicated to have significant biogenic magnetite contents[6]. Late Palaeocene-early Eocene (LPEE) IRM distributions differ from those for early Palaeogene samples with biogenic magnetite (Fig. S11). Even considering that biogenic magnetite occurrences at Contessa Road have not been identified conclusively, we carried out an additional magnetic mineral unmixing assessment including biogenic magnetite to test its influence in our data (right column in Fig. S10). We separated low coercivity biogenic magnetite, with B_c values >30-40 mT, from detrital maghemite and magnetite, which have overlapping B_c values <30 mT[7-9]. Most samples were fitted with these components and a high coercivity component; however, the early Eocene terrigenous zone (EETZ) sample required an additional component with a B_c value of 80 mT, which may be related to maghemitized magnetite and/or "giant" biogenic magnetite crystals, which have not been identified at Contessa Road[8,9]. We identify that even if biogenic magnetite is present in the LPEE Contessa Road record, the IRM unmixing component associated with detrital magnetite and maghemite would have larger proportions than biogenic magnetite (Fig. S12). These results validate our interpretations about the detrital origin of LPEE Contessa Road magnetic minerals.

Bulk-rock (BR) magnetic mineral concentrations increase during short-lived carbon cycle perturbations; however, the highest concentrations are identified across the early Eocene terrigenous zone (EETZ). These patterns suggest that the BR concentration parameters indicate calcium carbonate ($CaCO_3$) dissolution (Fig. S4; see Results and Discussion). Major high and low coercivity components have clear visual similarities with the HIRM and ARM records, respectively (Fig. S4, S8). This indicates that HIRM does not underestimate or overestimate haematite concentrations in high coercivity magnetic mineral assemblages, and that ARM is suitable for estimating maghemite and magnetite contents in low coercivity assemblages.

Carbonate free basis (CFB) magnetic mineral concentration parameters follow similar patterns compared to saturation remanent magnetization (M_{rs}-CFB; See Results), HIRM-CFB, and ARM-CFB (Fig. S8; see Results). This confirms that CFB rock magnetic concentration parameters (Fig. 5) reflect detrital mineral inputs to Contessa Road. The coercive force (B_c) has clear visual similarities with coercivity of remanence (B_{cr}) and S-ratio patterns, which confirms that they reveal compositional variability of high and low coercivity minerals (Fig. S9). The L-ratio also has a similar pattern to B_c, B_{cr}, and S-ratio, which indicates dominantly high coercivity mineral occurrences across some carbon cycle perturbations. L-ratio values for EELMZ carbonates verify rock magnetic results that suggest that this interval contains different magnetic minerals with respect to the rest of Contessa Road (Fig. S9d). High EELMZ L-ratio values may be related to goethite, which has not been identified in other Contessa Road intervals. There is no linear trend between L-ratio and HIRM (Fig. S17), which indicates that HIRM is a suitable haematite content indicator[10].

Supplementary discussion

The early Eocene low magnetization zone (EELMZ)

Whitish limestones in the EELMZ seem to suggest a bleaching process that is not identified in other parts of the LPEE Contessa Road section[1] (Fig. 5). A similar limestone bleaching interval is present in Scaglia Rossa carbonates just below the Cretaceous/Palaeogene (K/Pg) boundary. Abrajevitch et al.[11] interpreted the bleaching as due to ocean acidification produced by Deccan Traps volcanism, which caused magnetic mineral dissolution of pigmentary haematite that developed an interval similar to the EELMZ. If ocean acidification produced the EELMZ, extensive $CaCO_3$ dissolution would have been identified across this interval (Fig. 2b). Instead, it has high Ca/$CaCO_3$ contents and low detrital element values that do not indicate $CaCO_3$ dissolution (Fig. S3); therefore, this mechanism cannot explain the EELMZ. Reductive diagenesis, which can cause magnetic mineral dissolution and is associated with organic matter degradation via increased productivity[12], is not evident as there are no major low coercivity magnetic mineral content changes across the EELMZ (Fig. 5c). Furthermore, the presence of maghemite within this interval (Fig. 3, S5, S6) indicates insignificant reductive diagenesis.

Considering that ocean acidification and reductive diagenesis are not clearly related to EELMZ formation, compositional variation of terrigenous materials is a feasible explanation for EELMZ development. Although the EELMZ is indicated clearly by reduced M_{rs}-CFB and HIRM-CFB values, ARM-CFB and high-field magnetic susceptibility (χ_{hf})-CFB indicate that terrigenous inputs did not change substantially across the EELMZ at Contessa Road (Fig. 5a-c; Fig. S6a). These patterns suggest that the EELMZ only records a high coercivity magnetic mineral decrease, which may be associated with goethite rather than pigmentary haematite according to rock magnetic experiments (Fig. 3). This interpretation suggests hydroclimate variation following the ETM 3 from dry-drier hydroclimates to wet conditions, which indicates that our $PC1_{arid}$ index cannot be used across the EELMZ (Fig. 9; see Discussion). Post-depositional infiltration of reducing waters across EELMZ limestones is a further mechanism that could have controlled magnetic mineral dissolution in Contessa Road carbonates[13]. This process cannot be ruled out as a possible EELMZ formation mechanism and does not necessarily imply a hydroclimate shift in the western Tethys; therefore, the origins and regional significance of the EELMZ cannot be indicated conclusively. Future research on similar records of LPEE limestone bleaching could help to indicate the origin of the Contessa Road EELMZ.

Supplementary tables and figures

Climate-related acronyms	
Meaning	**Acronym**
Shared socio-economic pathway	SSP
Intergovernmental Panel on Climate Change	IPCC
Late Palaeocene-early Eocene	LPEE
Palaeocene-Eocene Thermal Maximum	PETM
Eocene Thermal Maximum 2	ETM 2
Eocene Thermal Maximum 3	ETM 3
Geochemistry-related acronyms	
Meaning	**Acronym**
Stable oxygen isotopes	$\delta^{18}O$
Stable carbon isotopes	$\delta^{13}C$
Carbon isotope excursions	CIE
Calcium carbonate	$CaCO_3$
Rock magnetism-related acronyms	
Meaning	**Acronym**
Bulk-rock	Br
Carbonate free basis	CFB
Saturation remanent magnetization	M_{rs}
Saturation magnetization	M_s
Hard isothermal remanent magnetization	HIRM
Anhysteretic remanent magnetization	ARM
Magnetic susceptibility	χ
Low-field magnetic susceptibility	χ_{lf}
High-field magnetic susceptibility	χ_{hf}
Coercivity	B_c
Coercivity of remanence	B_{cr}
Other acronyms	
Meaning	**Acronym**
Scanning electron microscope	SEM
Energy dispersive X-ray spectroscopy	EDXS
Principal component analysis	PCA
Locally estimated scatterplot smoothing	LOESS
New acronyms introduced in this manuscript	
Meaning	**Acronym**
Early Eocene terrigenous zone	EETZ
Early Eocene low magnetization zone	EELMZ

Tab. S1. **Acronyms.** List of the acronyms used.

PCA_{dis}		
Variable	**Loading $PC1_{dis}$**	**Loading $PC2_{dis}$**
Ca	-0.39	0.47
Fe	0.44	0.02
Rb	0.41	-0.26
Si	0.35	0.84
Ti	0.40	0.02
Zr	0.43	-0.05
PC_{all}		
Variable	**Loading $PC1_{all}$**	**Loading $PC2_{all}$**
Ca	-0.12	-0.41
Fe	0.22	0.35
Rb	0.14	0.42
Si	0.19	0.25
Sr	0.02	-0.03
Ti	0.21	0.29
Zr	0.19	0.36
CFB-χ_{lf}-χ_{hf}	0.29	-0.13
CFB-χ_{lf}	0.31	-0.11
CFB-χ_{hf}	0.23	0.01
CFB-M_s	0.30	-0.13
CFB-M_{rs}	0.31	-0.12
CFB-HIRM	0.29	-0.04
CFB-ARM	0.26	-0.16
CFB-LCC	0.28	-0.12
CFB-HCC	0.29	-0.13
B_{cr}	-0.18	0.27
S-ratio	0.16	-0.26
PCA_{arid}		
Variable	**Loading $PC1_{arid}$**	**Loading $PC2_{arid}$**
CFB-ARM	0.49	0.08
B_{cr}	-0.45	0.46
S-ratio	0.41	-0.55
CFB-HIRM	0.39	0.61
CFB-M_{rs}	0.48	0.34

Tab. S2. **Principal component analysis (PCA) loadings.** PCA loadings of the variables used for PC_{dis}, PC_{all} and PC_{arid}.

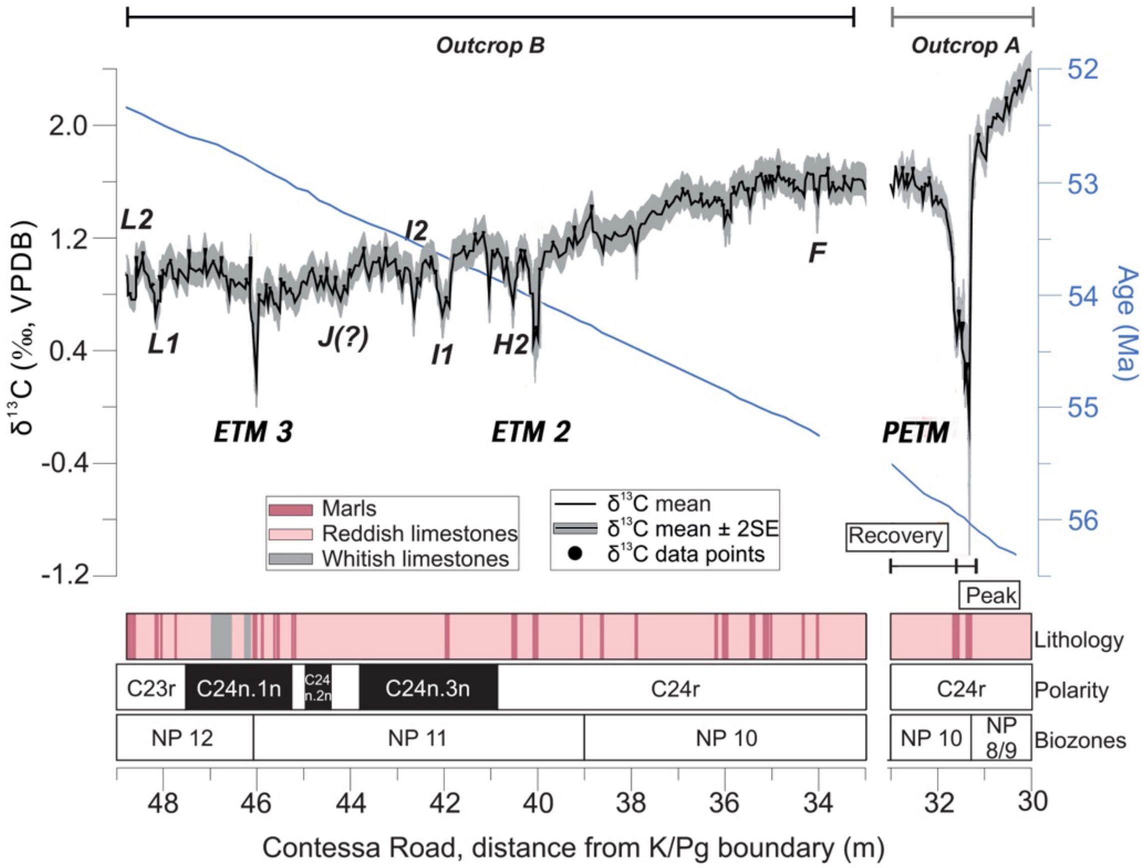

Fig. S1. **Stratigraphic framework for the Contessa Road section.** Stable carbon isotopes ($\delta^{13}C$) for outcrops A and B. Lithology is indicated at the bottom of the figure: reddish limestones (pink), marls (red), and whitish limestones (grey). The magnetostratigraphy (black/white = normal/reversal polarity) and biostratigraphy (calcareous nannofossil zones[1,14]) are also presented. The age model for this section (depth versus age) is indicated by blue lines[15]. $\delta^{13}C$ is presented in terms of the mean (black) ± 2 standard errors (2SE, grey bands). Hyperthermals (Palaeocene-Eocene Thermal Maximum (PETM), Eocene Thermal Maximum (ETM) 2 and ETM 3), smaller carbon cycle perturbations, and PETM peak (initial phase) and recovery phases are also indicated.

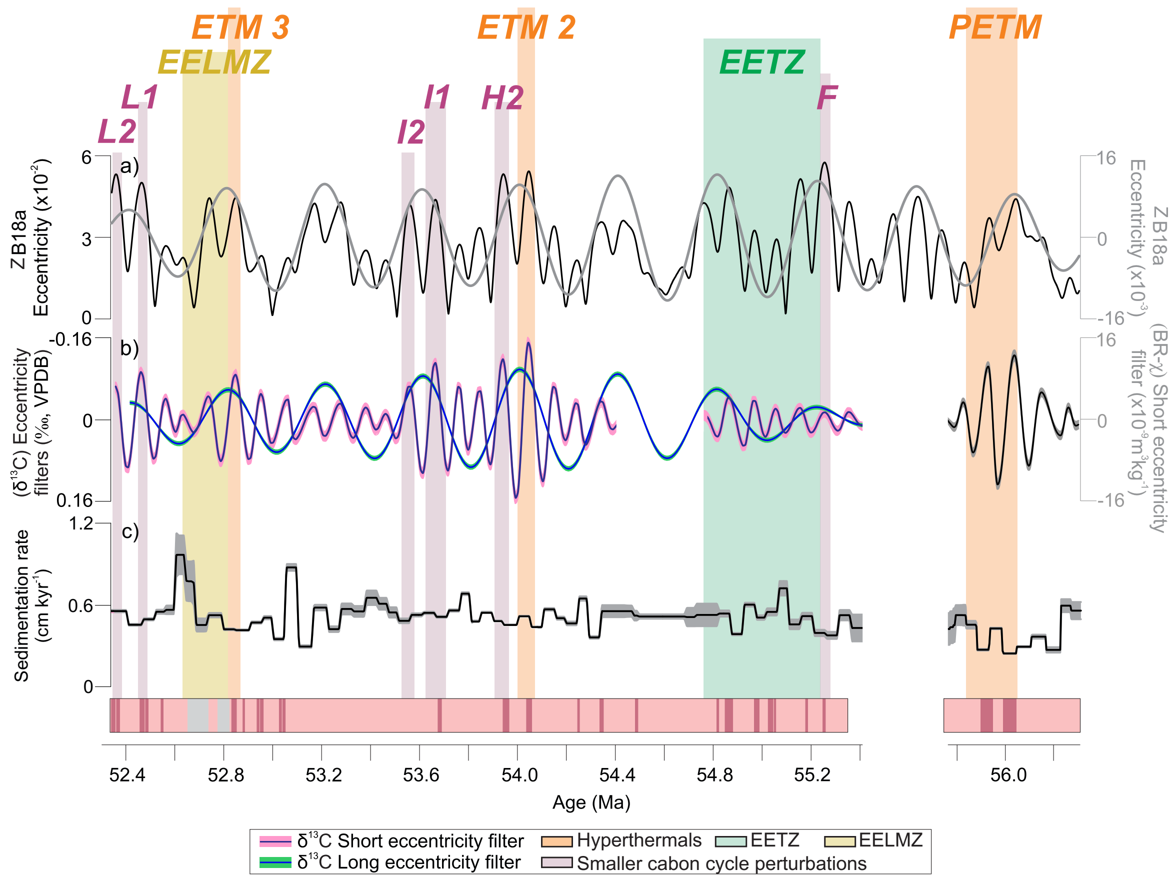

Fig. S2. **Astrochronological age model for the Contessa Road section.** (a) Short eccentricity (black) and long eccentricity (grey) signals from the ZB18a orbital solution[16]. (b) Contessa Road short eccentricity signals of bulk-rock magnetic susceptibility (BR-χ) (mean in black ± 2 standard errors (2SE) in grey), and Contessa Road long (mean in blue ± 2SE in green) and short eccentricity signals of stable carbon isotope ($\delta^{13}C$) records (mean in blue ± 2SE in pink)[15]. (c) Contessa Road sedimentation rates presented in terms of mean (black) ± 2SE (shaded grey bands)[15]. Hyperthermals (Palaeocene-Eocene Thermal Maximum (PETM), Eocene Thermal Maximum (ETM) 2 and ETM 3), smaller carbon cycle perturbations, the early Eocene terrigenous zone (EETZ), and the early Eocene low magnetization zone (EELMZ) are indicated with orange, purple, green, and yellow bands, respectively. Lithology is presented at the bottom of the figure with reddish (pink) and whitish limestones (grey) and marls (red).

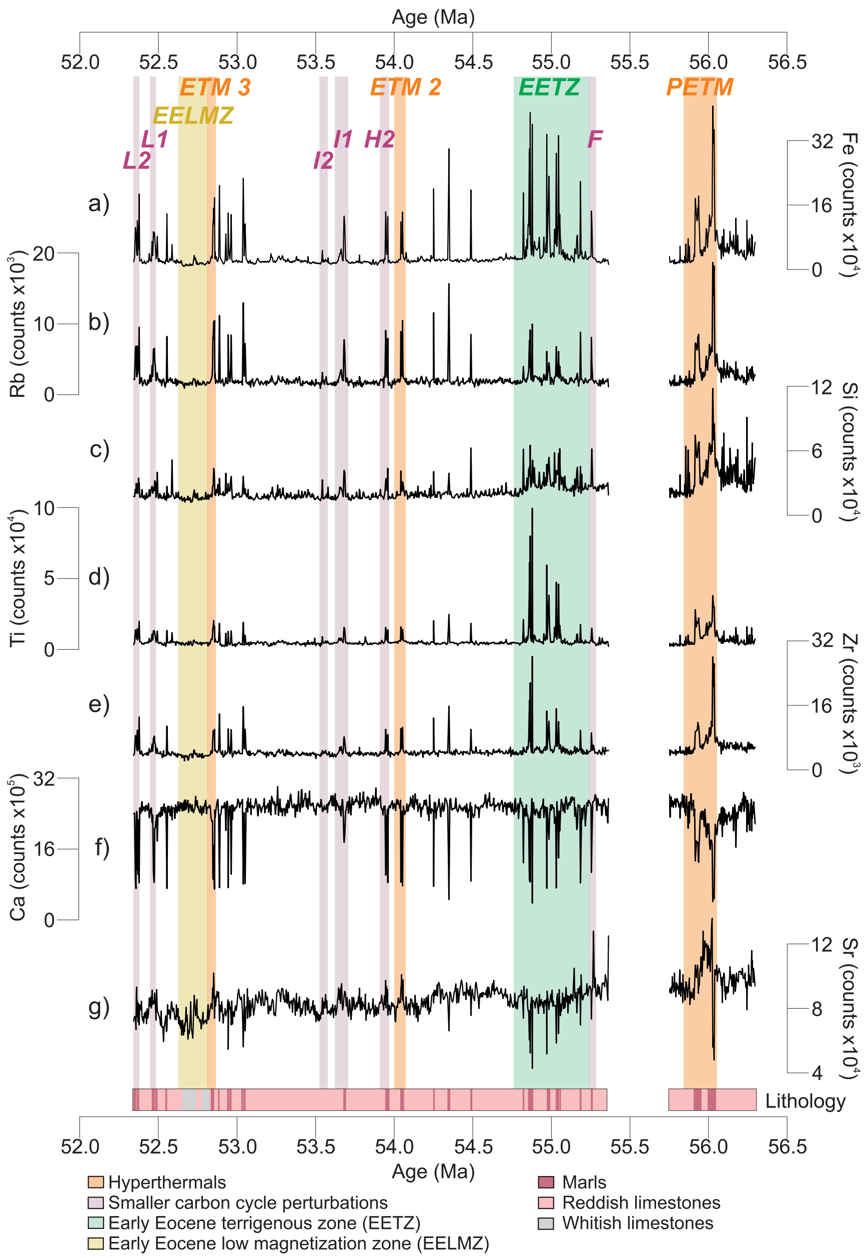

Fig. S3. **X-ray fluorescence (XRF) records.** Contessa Road (a) Fe, (b), Rb, (c) Si, (d) Ti, (e) Zr, (f) Ca, and (g) Sr records. Lithology is indicated at the bottom of the figure with reddish (pink) and whitish limestones (grey) and marls (red). Hyperthermals (Palaeocene-Eocene Thermal Maximum (PETM), Eocene Thermal Maximum (ETM) 2 and ETM 3), smaller carbon cycle perturbations, the early Eocene terrigenous zone (EETZ), and the early Eocene low magnetization zone (EELMZ) are indicated with orange, purple, green, and yellow bands, respectively. Source data are provided as a Source Data file.

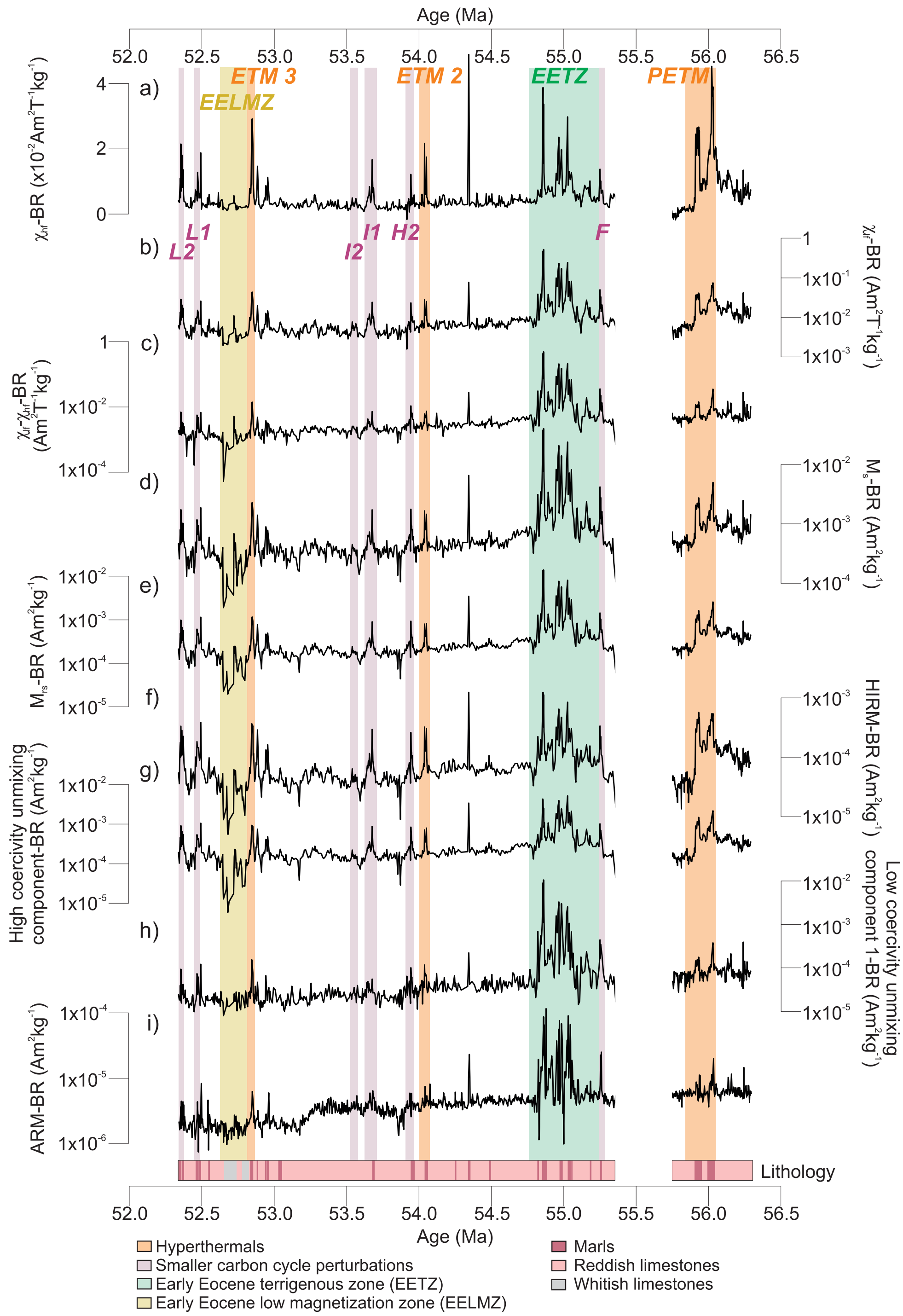

Fig. S4. **Bulk-rock (BR) magnetic mineral concentration parameters for the Contessa Road section.** (a) high-field magnetic susceptibility (χ_{hf})-BR, (b) low-field magnetic susceptibility (χ_{lf})-BR, (c) χ_{lf}-χ_{hf}-BR, (d) saturation magnetization (M_s)-BR, (e) saturation remanent magnetization (M_{rs})-BR, (f) hard isothermal remanent magnetization (HIRM)-BR, (g) high coercivity unmixing component-BR, (h) low coercivity unmixing component 1-BR (main low coercivity unmixing component), and (i) anhysteretic remanent magnetization (ARM)-BR. Lithology is presented at the bottom of the figure with reddish (pink) and whitish limestones (grey) and marls (red). Hyperthermals (Palaeocene-Eocene Thermal Maximum (PETM), Eocene Thermal Maximum (ETM) 2 and ETM 3), smaller carbon cycle perturbations, the early Eocene terrigenous zone (EETZ), and the early Eocene low magnetization zone (EELMZ) are indicated with orange, purple, green, and yellow bands, respectively. Source data are provided as a Source Data file.

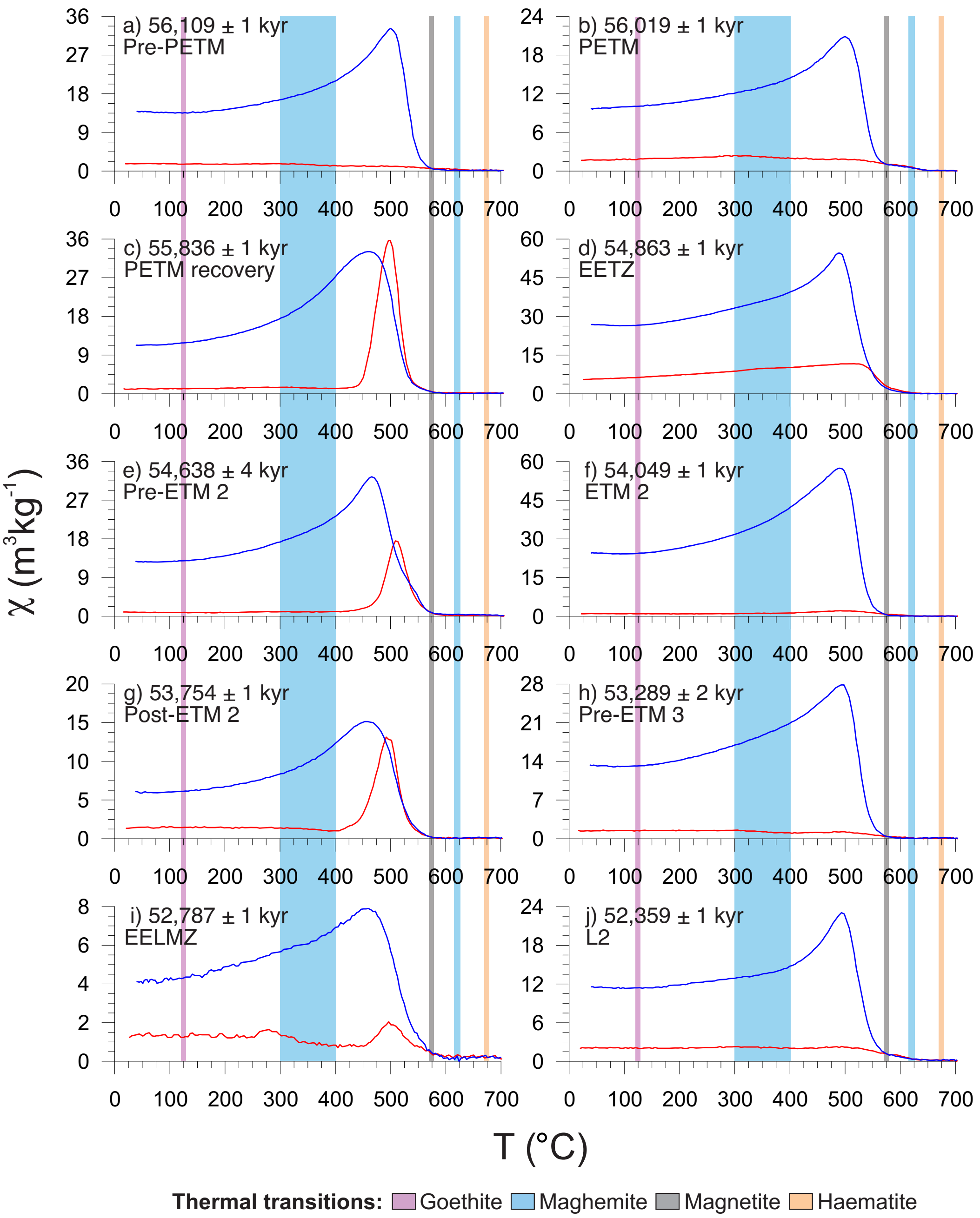

Fig. S5. **χ-T curves.** The cooling (blue) and heating (red) curves in χ-T experiments are presented for samples from (a) pre-Palaeocene-Eocene Thermal Maximum (PETM), (b) PETM, (c) PETM recovery, (d) early Eocene terrigenous zone (EETZ), (e) pre-Eocene Thermal Maximum 2 (ETM 2), (f) ETM 2, (g) post-ETM 2, (h) pre-Eocene Thermal Maximum 3 (ETM 3), (i) early Eocene low magnetization zone (EELMZ), and (j) L2. Thermal transitions for magnetic minerals are indicated by purple (goethite), blue (maghemite), grey (magnetite), and orange (haematite) bars that cross all plots.

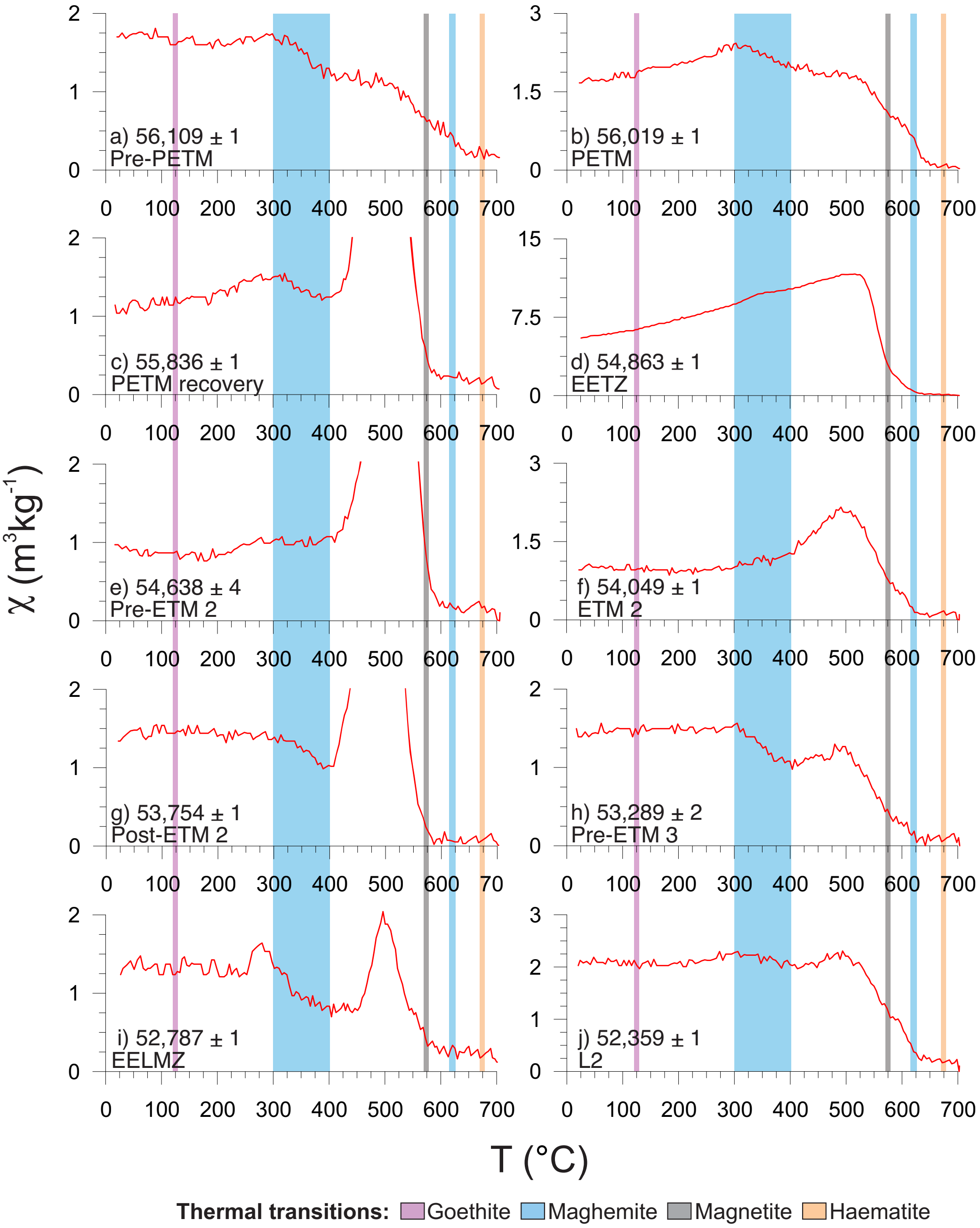

Fig. S6. **χ-T curves.** Heating (red) curves in χ-T experiments are presented for samples from (a) pre-Palaeocene-Eocene Thermal Maximum (PETM), (b) PETM, (c) PETM recovery, (d) early Eocene terrigenous zone (EETZ), (e) pre-Eocene Thermal Maximum 2 (ETM 2), (f) ETM 2, (g) post-ETM 2, (h) pre-Eocene Thermal Maximum 3 (ETM 3), (i) early Eocene low magnetization zone (EELMZ), and (j) L2. Thermal transitions for magnetic minerals are indicated by purple (goethite), blue (maghemite), grey (magnetite), and orange (haematite) bars that cross all plots.

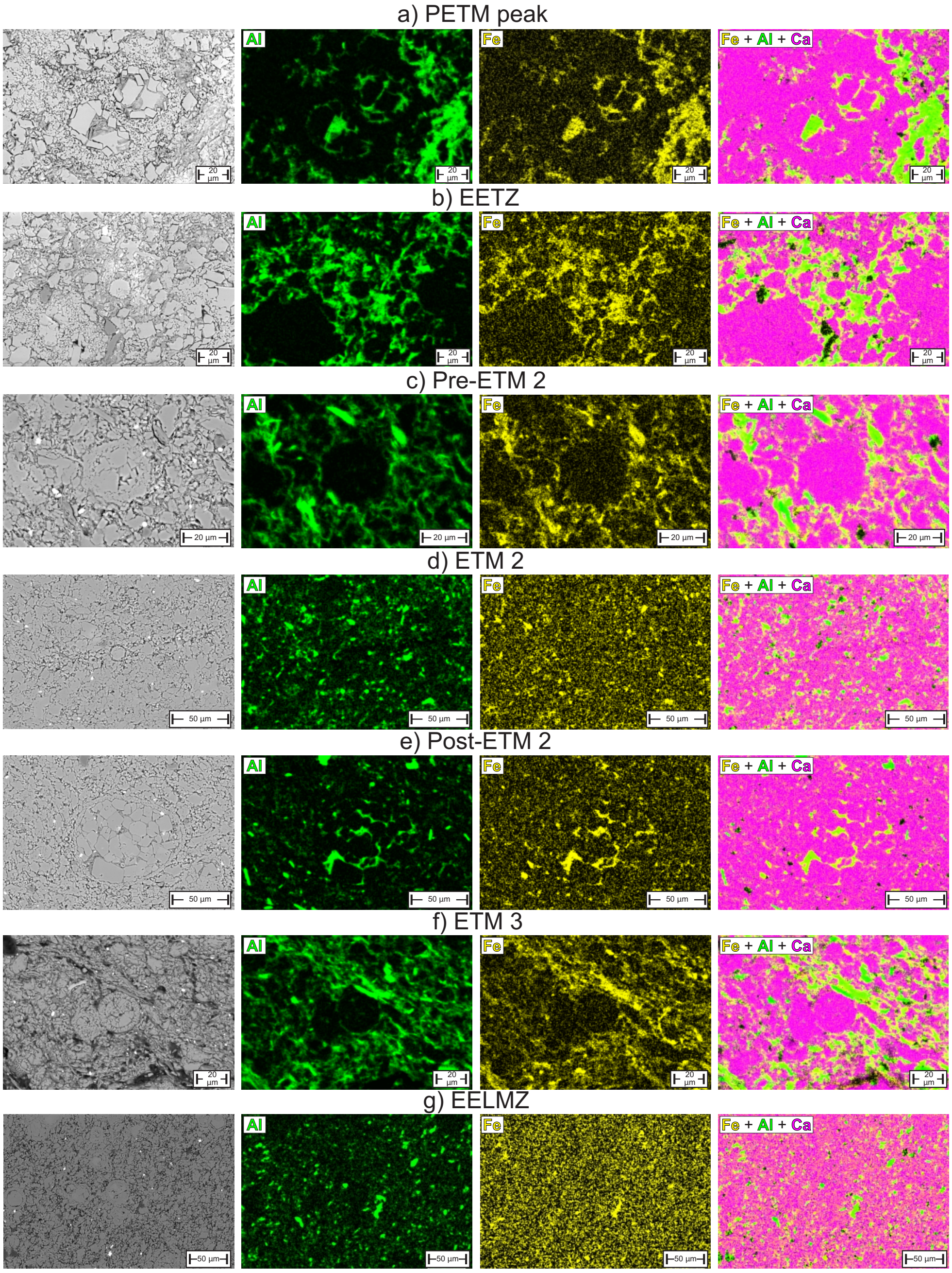

Fig. S7. **Scanning electron microscope (SEM) analyses.** SEM images obtained with a backscattered electron detector (left), with Al (green) and Fe (yellow) false-colour maps (centre), and Al (green), Fe (yellow), and Ca (pink) (right) maps for (a) the Palaeocene-Eocene Thermal Maximum (PETM) peak, (b) early Eocene terrigenous zone (EETZ), (c) pre-Eocene Thermal Maximum 2 (ETM 2), (d) ETM 2, (e) post-ETM 2, (f) Eocene Thermal Maximum 3 (ETM 3), and (g) early Eocene low magnetization zone (EELMZ).

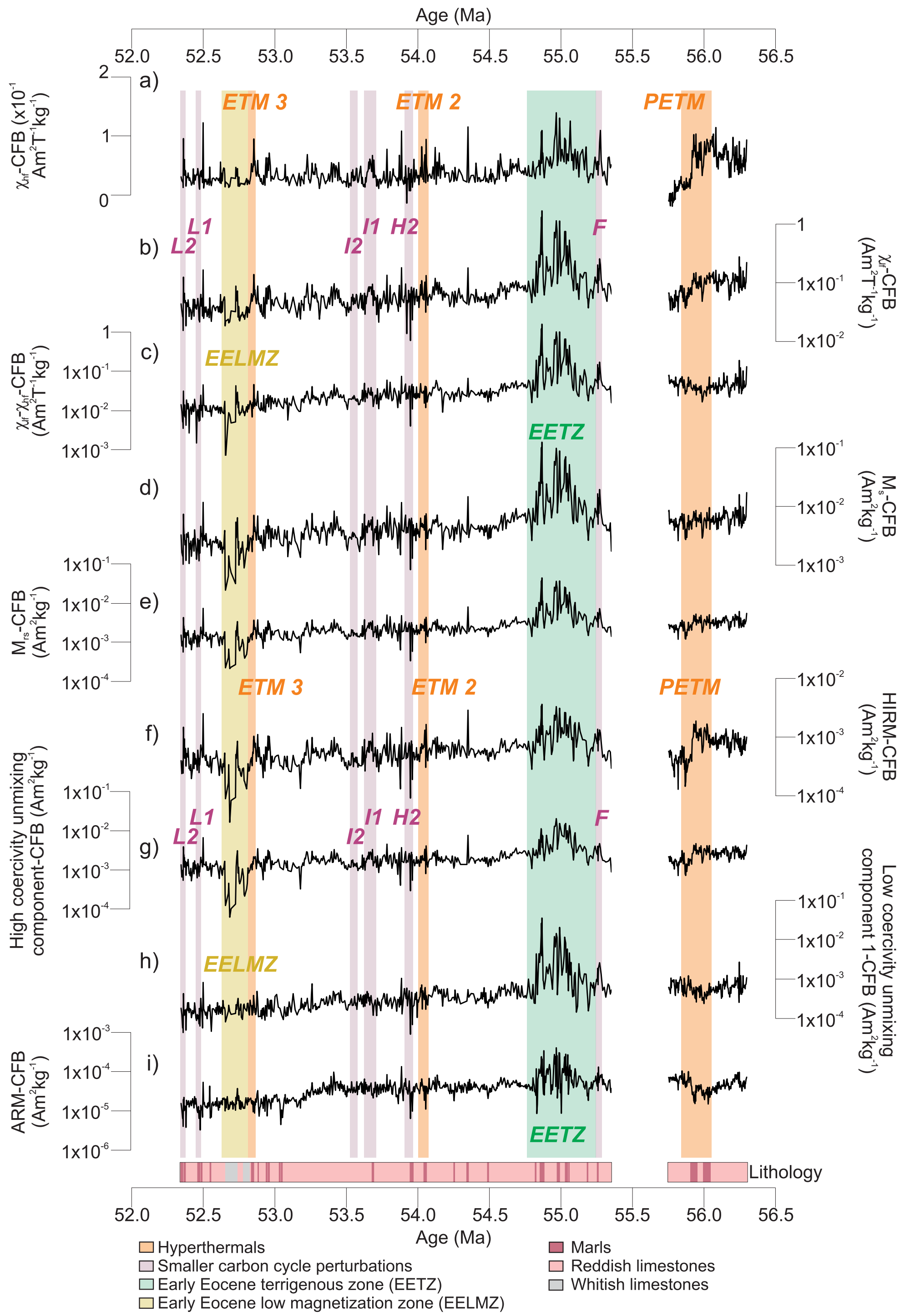

Fig. S8. **Carbonate free basis (CFB) magnetic mineral concentration parameters for the Contessa Road section.** (a) high-field magnetic susceptibility (χ_{hf})-CFB, (b) low-field magnetic susceptibility (χ_{lf})-CFB, (c) χ_{lf}-χ_{hf}-CFB, (d) saturation magnetization (M_s)-CFB, (e) saturation remanent magnetization (M_{rs})-CFB, (f) hard isothermal remanent magnetization (HIRM)- CFB, (g) high coercivity unmixing component- CFB, (h) low coercivity unmixing component 1-CFB (main low coercivity unmixing component), and (i) anhysteretic remanent magnetization (ARM)-CFB. Lithology is presented at the bottom of the figure with reddish (pink) and whitish limestones (grey) and marls (red). Hyperthermals (Palaeocene-Eocene Thermal Maximum (PETM), Eocene Thermal Maximum (ETM) 2 and ETM 3), smaller carbon cycle perturbations, the early Eocene terrigenous zone (EETZ), and the early Eocene low magnetization zone (EELMZ) are indicated with orange, purple, green, and yellow bands, respectively. Source data are provided as a Source Data file.

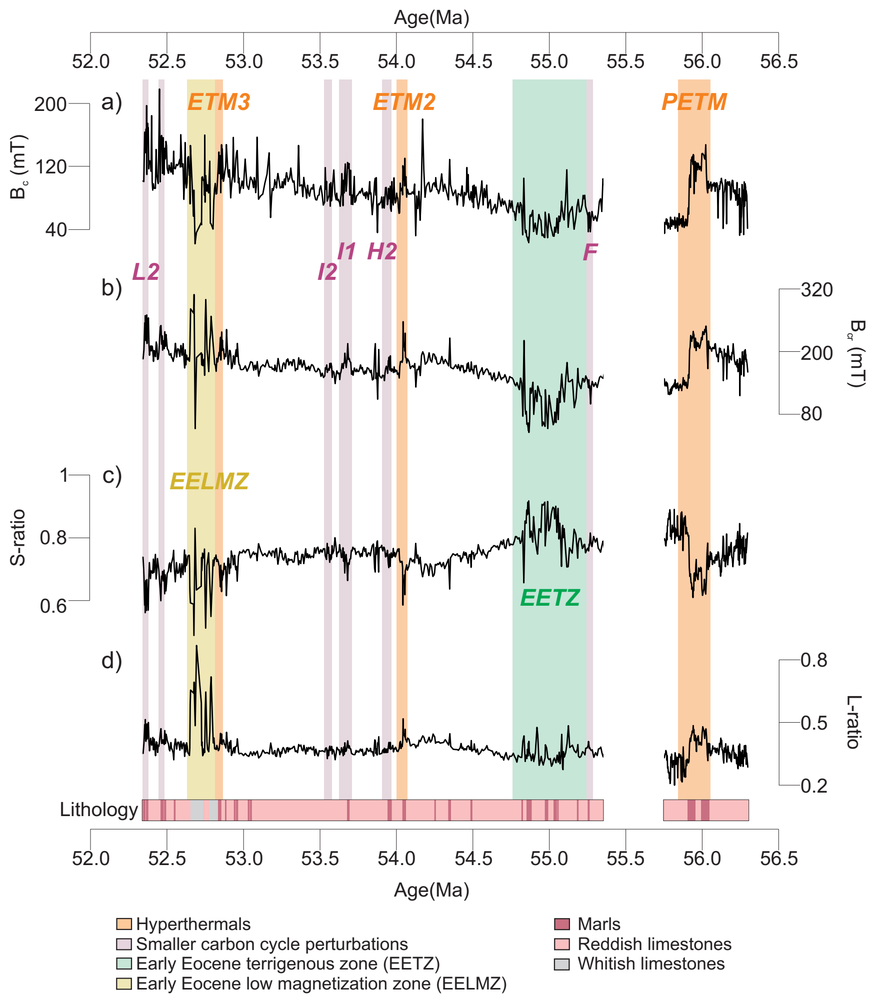

Fig. S9. **Magnetic mineral compositional parameters for the Contessa Road section.** (a) coercivity (B_c), (b) coercivity of remanence (B_{cr}), (c) S-ratio, and (d) L-ratio records. Lithology is presented at the bottom of the figure with reddish (pink) and whitish limestones (grey) and marls (red). Hyperthermals (Palaeocene-Eocene Thermal Maximum (PETM), Eocene Thermal Maximum (ETM) 2 and ETM 3), smaller carbon cycle perturbations, the early Eocene terrigenous zone (EETZ), and the early Eocene low magnetization zone (EELMZ) are indicated with orange, purple, green, and yellow bands, respectively. Source data are provided as a Source Data file.

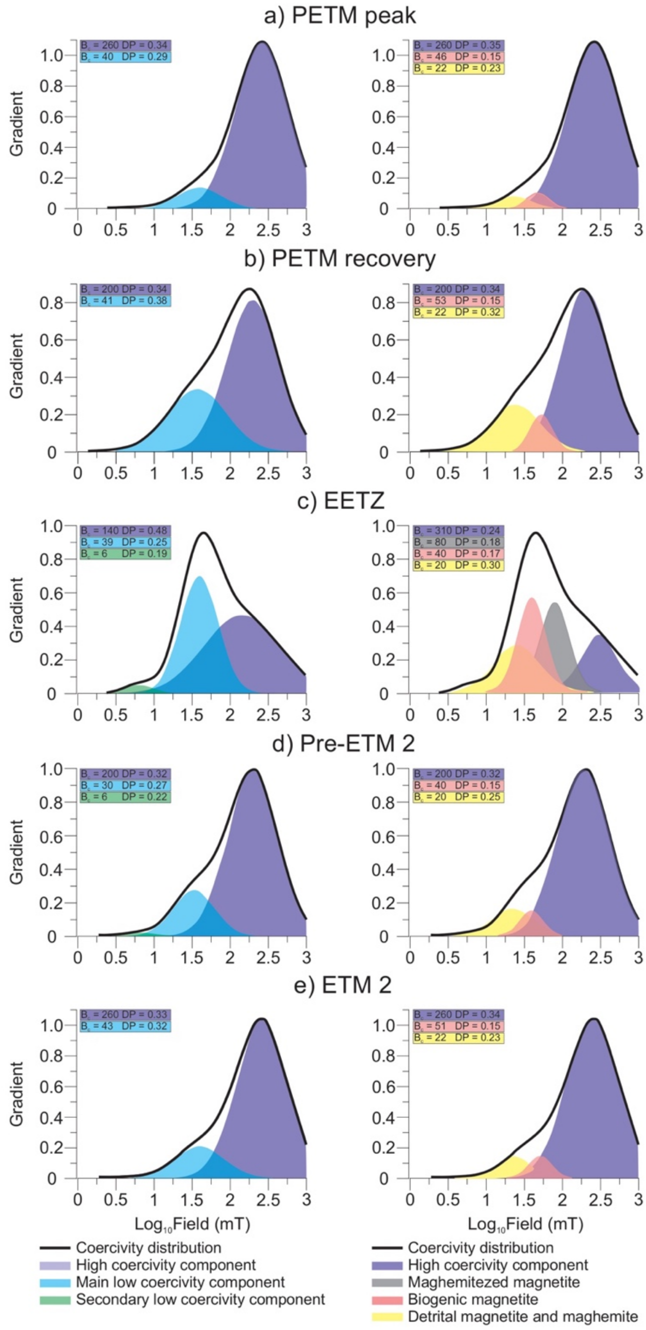

Fig. S10. **Isothermal remanent magnetization (IRM) distributions.** The left column indicates magnetic mineral unmixing assessments for three components that include a major high coercivity component (purple), a main low coercivity component (blue), and a residual smaller low coercivity component (green). These assessments were used to isolate the coercivity components presented in Fig. S4 and Fig. S8. These data also provided the records for principal component analysis of all data (Fig. 6b). The right column represents additional magnetic mineral unmixing assessments including a high coercivity component (purple), a biogenic magnetite component (orange), and a detrital magnetite/maghemite component (yellow). An additional component with intermediate coercivities (grey) also occasionally appears. Representative plots include samples from the (a) Palaeocene-Eocene Thermal Maximum (PETM) peak, (b) PETM recovery, (c) early Eocene terrigenous zone (EETZ), (d) pre-Eocene Thermal Maximum 2 (ETM 2), and (e) ETM 2. Coercivity (B_c) and dispersion parameter (DP) values are indicated within rectangles that have the same colour for each component.

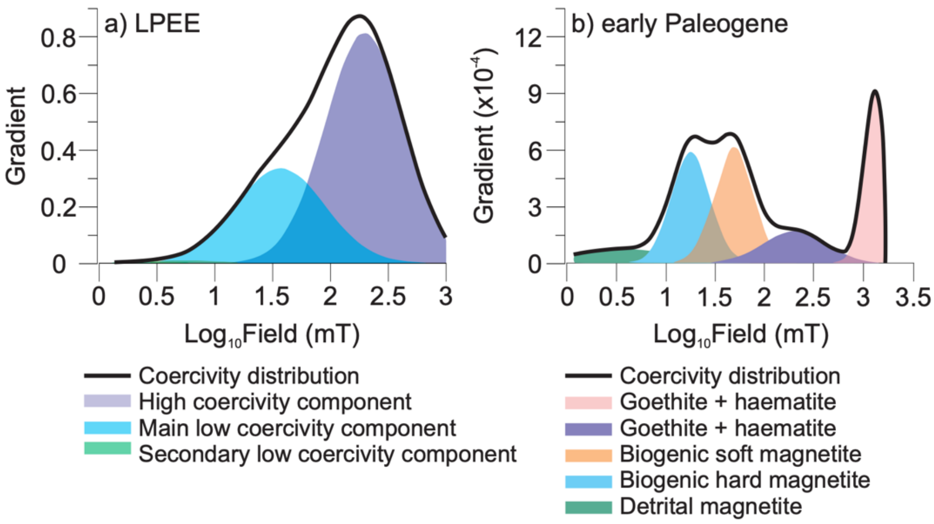

Fig. S11. **Magnetic mineral unmixing comparison.** Isothermal remanent magnetization (IRM) distributions for (a) late Palaeocene-early Eocene (LPEE) (present study) and (b) early Palaeogene Contessa Road samples[6].

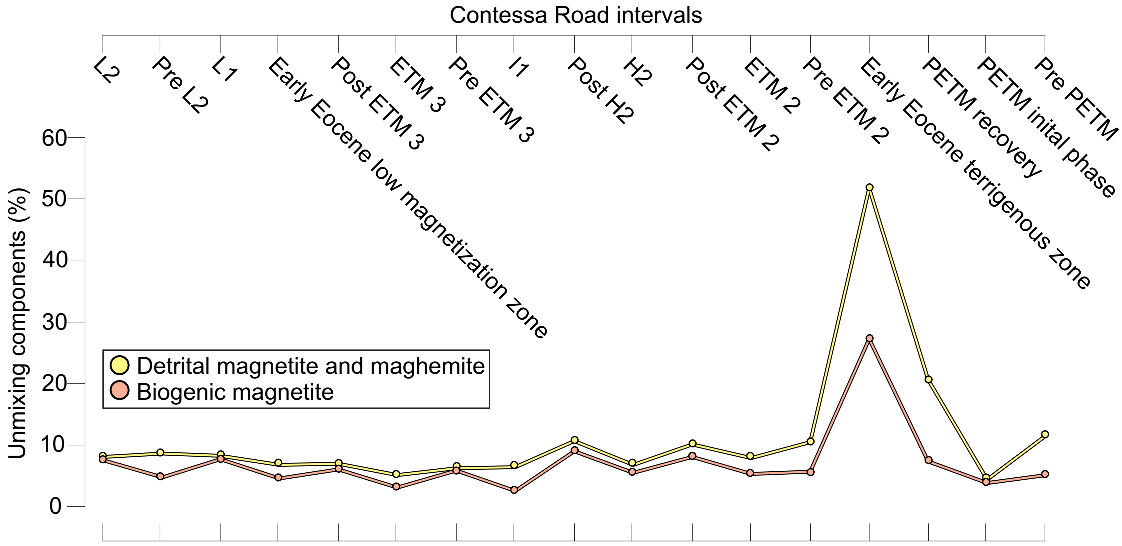

Fig. S12. **Magnetic mineral unmixing results.** Detrital magnetite/maghemite (yellow) and biogenic magnetite (orange) proportions from magnetic mineral unmixing results presented in the right panel of Fig. S10. Abbreviations were used for the Palaeocene-Eocene Thermal Maximum (PETM), Eocene Thermal Maximum (ETM) 2 and ETM 3.

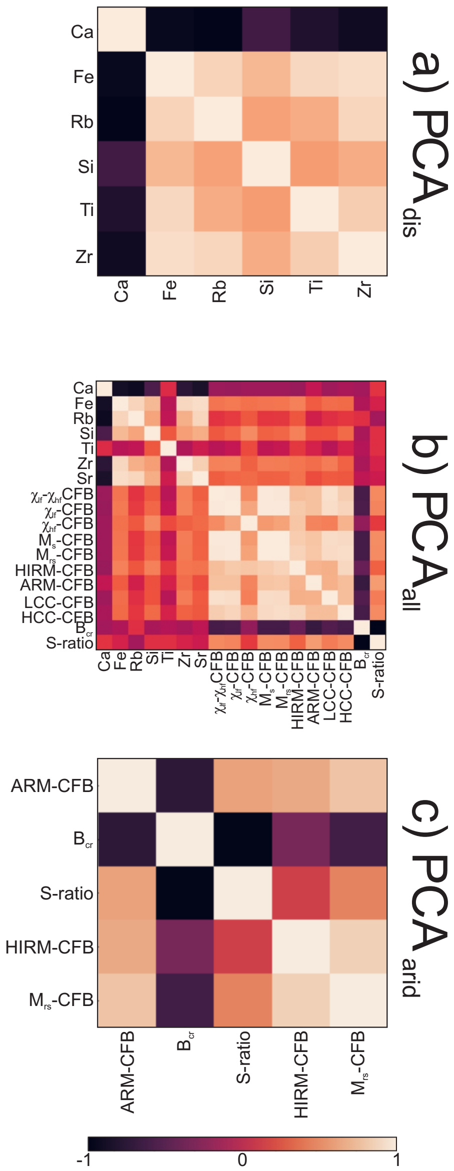

Fig. S13. **Principal component analysis (PCA).** Correlation matrices for (a) PCA_{dis}, (b) PCA_{all}, and (c) PCA_{arid}. Abbreviations were used for carbonate free basis (CFB), high-field magnetic susceptibility-CFB (χ_{hf}-CFB), low-field magnetic susceptibility-CFB (χ_{lf}-CFB), saturation magnetization-CFB (M_s-CFB), saturation remanent magnetization-CFB (M_{rs}-CFB), hard isothermal remanent magnetization-CFB (HIRM-CFB), high coercivity unmixing component-CFB (HCC-CFB), low coercivity unmixing component 1-CFB (main low coercivity unmixing component) (LCC-CFB), anhysteretic remanent magnetization-CFB (ARM-CFB), and coercivity of remanence (B_{cr}).

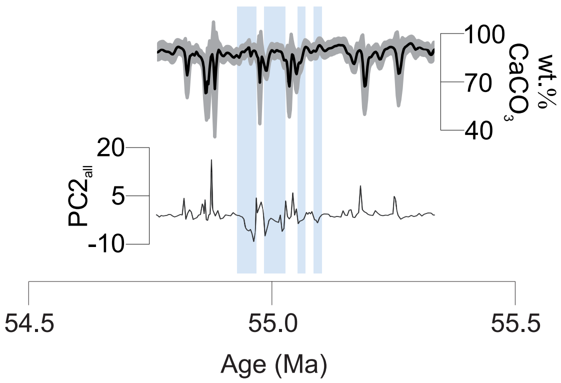

Fig. S14. **The early Eocene terrigenous zone (EETZ).** $CaCO_3$ (mean in black ± 2 standard errors (2SE) in gray) and $PC2_{all}$ comparison for the EETZ. Blue bands represent the negative $PC2_{all}$ peaks that coincide with high $CaCO_3$ values.

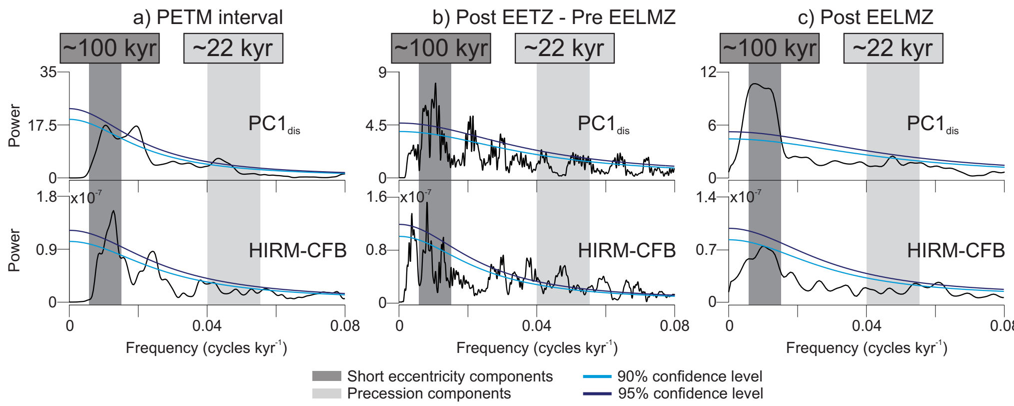

Fig. S15. **Spectral analysis.** Multi-taper power spectra for $PC1_{dis}$ and hard isothermal remanent magnetization in a carbonate free basis (HIRM-CFB) for different Contessa Road intervals. (a) The Palaeocene-Eocene Thermal Maximum (PETM), (b) the post early Eocene terrigenous zone-pre early Eocene low magnetization zone (post EETZ-Pre EELMZ) and (c) the post early Eocene low magnetization zone (EELMZ) define the intervals in which spectral analyses were carried out. Sky blue and dark blue lines indicate 90% and 95% confidence levels, respectively. Associated frequencies of short eccentricity and precession are indicated by dark grey and light grey bands, respectively. Short eccentricity (~100 kyr) and precession (~22 kyr) periods are related to spectral peaks over the 90%-95% confidence levels.

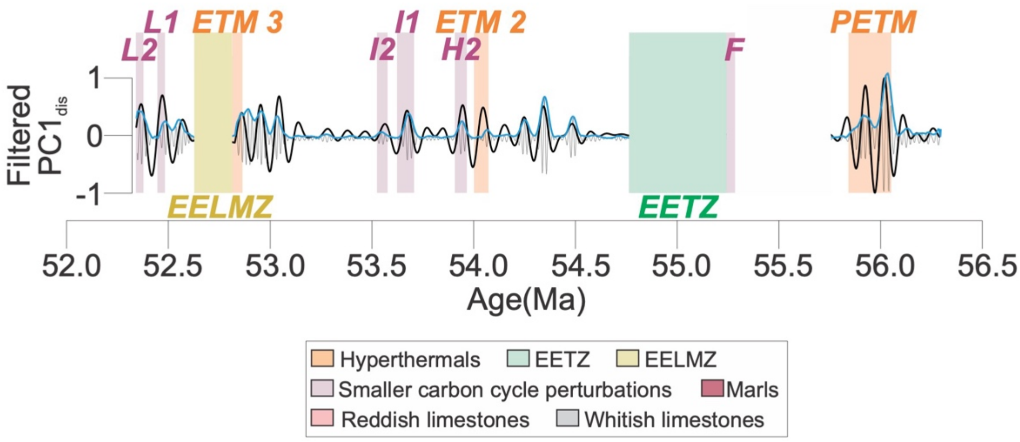

Fig. S16. **Amplitude modulation of precession.** $PC1_{dis}$ precession (grey) and its amplitude modulation patterns (blue) compared to the $PC1_{dis}$ short eccentricity signal. Hyperthermals (Palaeocene-Eocene Thermal Maximum (PETM), Eocene Thermal Maximum (ETM) 2 and ETM 3), smaller carbon cycle perturbations, the early Eocene terrigenous zone (EETZ), and the early Eocene low magnetization zone (EELMZ) are indicated with orange, purple, green, and yellow bands, respectively.

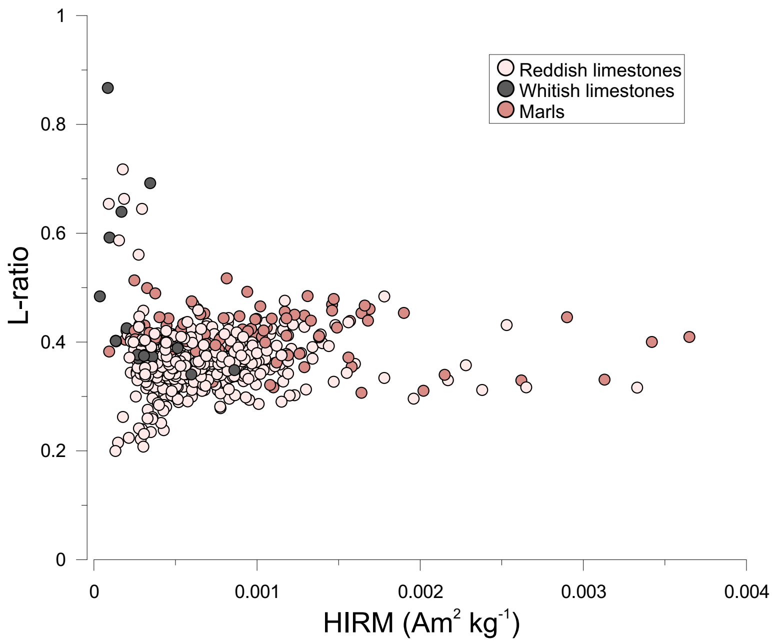

Fig. S17. **Hard isothermal remanent magnetization (HIRM) versus L-ratio for the Contessa Road section.** HIRM-L-ratio plot. Reddish limestones, whitish limestones, and marls are indicated by pink, grey, and red dots, respectively. Source data are provided as a Source Data file.

Supplementary references

1. Galeotti, S. *et al*. Orbital chronology of Early Eocene hyperthermals from the Contessa Road section, central Italy. *Earth Planet. Sci. Lett.* **290**, 192-200 (2010).
2. Piedrahita, V. A. *et al*. Orbital phasing of the Paleocene-Eocene Thermal Maximum. *Earth Planet. Sci. Lett.* **598**, 117839 (2022).
3. Francescone, F. *et al*. A 9 million-year-long astrochronological record of the early-middle Eocene corroborated by seafloor spreading rates. *Geol. Soc. Am. Bull.* **131**, 499-520 (2018).
4. Croudace, I. W., Rothwell, R. G. (Eds.), XRF Studies of Sediment Cores. Springer, Developments in Paleoenvironmental Research Series **17**, Dordrecht (2015).
5. Roberts, A. P. *et al*. Hematite (α-Fe_2O_3) quantification in sedimentary magnetism: limitations of existing proxies and ways forward. *Geosci. Lett.* **7**, 8 (2020).
6. Coccioni, R. *et al*. Paleoenvironmental signature of the Selandian-Thanetian transition event (STTE) and Early Late Paleocene Event (ELPE) in the Contessa Road section (western Neo-Tethys). *Palaeogeogr. Palaeoclimatol. Palaeoecol*. **523**, 62-77 (2019).
7. Liu, Y., Kissel, C., Mazaud, A., Pan, Y. & Li, J. Glacial-interglacial circulation and climatic changes in the South Indian Ocean (Kerguelen Plateau region) recorded by detrital and biogenic magnetic minerals. *J. Geophys. Res. Solid Earth* **128**, p.e2023JB027741 (2023).
8. Egli, R. Characterization of Individual Rock Magnetic Components by Analysis of Remanence Curves, 1. Unmixing Natural Sediments. *Stud. Geophys. Geod.* **48**, 391-446 (2004).
9. Wagner, C. L., Egli, R., Lascu, I., Lippert, P. C., Livi, K. J. T. & Sears, H. B. In situ magnetic identification of giant, needle-shaped magnetofossils in Paleocene–Eocene Thermal Maximum sediments. *Proc. Natl Acad. Sci.* **118**, e2018169118. (2021).
10. Liu, Q., Roberts, A. P., Torrent, J., Horng, C. S. & Larrasoaña, J. C. What do the HIRM and S-ratio really measure in environmental magnetism? *Geochem. Geophys. Geosyst.* **8**, Q09011 (2007).

11. Abrajevitch, A., Font, E., Florindo, F. & Roberts, A. P. Asteroid impact vs. Deccan eruptions: the origin of low magnetic susceptibility beds below the Cretaceous-Paleogene boundary revisited. *Earth Planet. Sci. Lett.* **430**, 209-223 (2015).
12. Roberts, A. P. Magnetic mineral diagenesis. *Earth-Sci. Rev.* **151**, 1-47 (2015).
13. Lowrie, W., Alvarez, W. & Asaro, F. The origin of the white beds below the Cretaceous-Tertiary boundary in the Gubbio section, Italy. *Earth Planet. Sci. Lett.* **98**, 303-312 (1990).
14. Giusberti, L., Coccioni, R., Sprovieri, M. & Tateo, F. Perturbation at the sea floor during the Paleocene-Eocene Thermal Maximum: evidence from benthic foraminifera at Contessa Road, Italy. *Mar. Micropaleontol.* **70**, 102-119 (2009).
15. Piedrahita, V. A. *et al*. Accelerated light carbon sequestration following late Paleocene-early Eocene carbon cycle perturbations. *Earth Planet. Sci. Lett.* **604**, 117992 (2023).
16. Zeebe, R. E. & Lourens, L. J. Solar system chaos and the Paleocene-Eocene boundary age constrained by geology and astronomy. *Science* **365**, 926-929 (2019).